*Antarctic Science 21(6), 619–631 (2009)* © Antarctic Science Ltd 2009 doi:10.1017/S0954102009990289

# An approach to quantifying Pliocene ice sheet dynamics via slope failure frequencies recorded in Antarctic Peninsula rise sediments

**DANIEL A. HEPP* and TOBIAS MÖRZ**

*MARUM – Center for Marine Environmental Sciences and Department of Geosciences, University of Bremen, PO Box 330440, 28334 Bremen, Germany*
**dhepp@uni-bremen.de*

**Abstract:** Understanding of glacially driven sedimentary transport systems across the shelf to the slope and subsequently to deep sea sediment bodies along the Pacific continental margin of Antarctic Peninsula is crucial for interpreting ice sheet dynamics. Here we quantify slope-failure frequencies recorded in Pliocene core intervals of ODP Site 1095. We used the relationship between long-term sedimentation rate and marine carbon burial efficiency to calculate glacial or interglacial specific sedimentation rates. Using the decompacted average length of glacial-interglacial cycles it was possible to solve a set of linear equations to derive average half-periods of 61.59 and 59.77 kyr respectively for the time interval 5.8–3.2 Ma. The resulting frequency distribution of slope failures reflects short and rapid but cyclic ice advances every ~375 years. Short retention times between slope loading and slope failure are supported by biogenic silica dissolution analyses. This study demonstrates the potential of the rise record to improve models of orbitally controlled size variations of the West Antarctic ice sheet and confirms the hypothesis of a highly dynamic ice sheet during the early Pliocene warm period.

Received 23 July 2008, accepted 11 May 2009

**Key words:** Drift 7, ODP Site 1095, opal leaching rate, sedimentation rate, turbidite frequency

## Introduction

### *Slope failure mechanisms along the Antarctic Peninsula continental margin*

Slope instabilities along ocean margins are the result of various geological processes such as plate tectonics, eustatic sea level variations, or erosion associated with slope loading. Sedimentary slope failures are the most important trigger mechanism for sediment gravity flows (e.g. turbidites; Løseth 1999).

Turbidites are common deep water deposits (Stow & Mayall 2000). Turbidity currents can be initiated on slopes by the transformation of slides and slumps into turbulent debris flows as they incorporate more water (Stow 1986, Løseth 1999). In numerical experiments using a multi-process sedimentation model, O'Grady & Syvitski (2001) showed that the type of mass movement depends on the failed sediment type. Sandy or silty material results in turbidite down-slope transport, whereas clayey materials lead to debris flows. The frequency with which turbidity currents are generated depends on source area, delivery system, slope and seismic activity.

Along the Pacific continental margin of the Antarctic Peninsula, the driving mechanisms for slope loading and failure are erosion of the shelf or hinterland by advancing ice sheets during glacials (Raymond 2002, Dowdeswell *et al*. 2004, Bart *et al*. 2007). The most rapid flow of the West Antarctic ice sheet occurs in areas of ice streams. They occupy glacial troughs, which are observed on the Antarctic Peninsula shelf (Fig. 1 location 1; Pudsey & Camerlenghi 1998, Rebesco *et al*. 2002) and around West Antarctica (Anderson *et al*. 2001). Ice stream flow velocities are typically a few hundred metres per year (Anderson *et al*. 2001). Elverhøi *et al*. (1998) compared sediment fluxes of ice streams with the sediment transport efficiency of large fluvial systems and demonstrated that glaciers are far more effective in terms of erosion than rivers. They compiled glacial erosion data from sediment budget and sediment yield studies from the Svalbard–Barents Sea region. According to this study, fast flowing ice streams have the potential to erode terrigenous material at rates more than 1 mm $yr^{-1}$.

Along the Pacific continental margin of the Antarctic Peninsula, the grounded ice streams (Fig. 1 location 2) transport eroded terrigenous material over the shelf edge to the over-steepened slope (Fig. 1 location 3; Rebesco *et al*. 1996). Frequent slope failures trigger turbidity currents, which run in channels (Fig. 1 location 4) between large elongated sediment bodies (Fig. 1 location 5) to the abyssal plain. The passage of large turbidity currents through channels (Diviacco *et al*. 2006) results in spill over silt lamina deposits on twelve sediment bodies along the

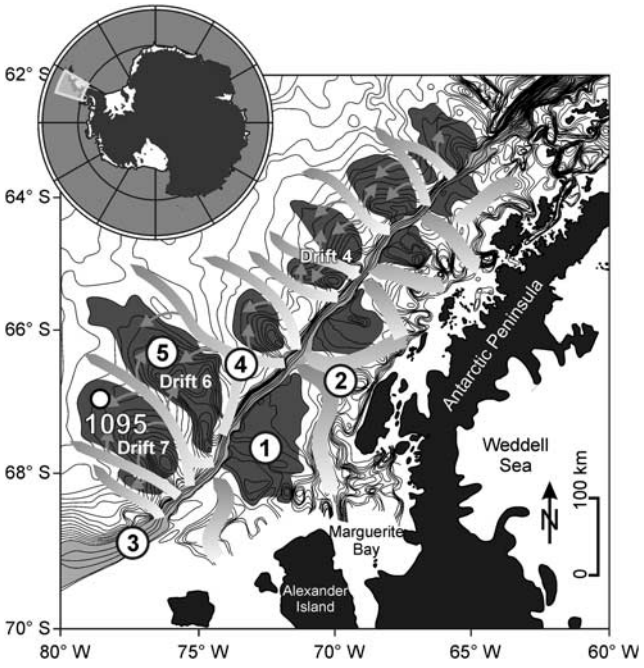


**Fig. 1.** Bathymetric map of the Pacific continental margin off the Antarctic Peninsula. The map shows a glacially driven sediment feeder system of 1) lobes and 2) troughs on the outer shelf, 3) an oversteepened slope, 4) deep sea channels, and 5) sediment drifts on the continental rise and the location of ODP Site 1095 on the distal part of Drift 7 (modified after Lucchi *et al*. 2002, Rebesco *et al*. 2002).

Antarctic continental rise. These sediment drifts were developed by a complex interplay of down-slope and along-slope processes. The origin of these so called 'drift bodies' is still a matter of controversy and depends on the relative importance given to both processes (McGinnis & Hayes 1995, Rebesco *et al*. 1996, 2002, Uenzelmann-Neben 2006).

An exception from the otherwise frequent, small scale glacially controlled turbidite events along the West Antarctic continental margin are two documented, large debris flow deposits between Drift 6 and 7 and within sediment Drift 4 (Fig. 1). These mega flow events are associated with catastrophic continental margin collapse in the late Pliocene (Diviacco *et al*. 2006, Rebesco & Camerlenghi 2008).

The interaction of ice volume evolution, slope loading and turbidity depositional processes plays a major role in drift build up during glacials and the subsequent deglaciation phase. On the passive and tectonically stable Pacific continental margin of the Antarctic Peninsula, the time interval between slope loading and slope failure mainly depends on slope angle and sediment type. The slope of the outer continental shelf is very steep with an average angle of 16°, making simple slope loading by the 'ice sheet feeder system' sufficient to trigger slope failure. This means that local slope instabilities along the Pacific margin of the Antarctic Peninsula are directly linked to regional ice events resulting in turbidity depositions on the drift. Mörz (2002) showed that the drift bodies represent the most proximal continuous sedimentary recorders for West Antarctic ice events and glacial-interglacial cyclicity.

### *Organic matter burial and preservation*

Organic carbon and biogenic silica ($BSiO_2$) are important components in the marine record. They are used as proxies for West Antarctic palaeoproductivity but are also prone to diagenetic recycling.

The burial efficiency of organic carbon in marine sediments is linked to the marine carbon cycle and plays a major role controlling atmospheric $CO_2$ and $O_2$ (Burdige 2006, pp. 408–441). Several factors control the preservation of organic matter in marine sediments, e.g. organic matter-mineral interactions, organic matter composition and reactivity, and the time of sediment oxygen 'exposure' (Burdige 2006). Typical recent open ocean deep sea sediment has organic carbon content as low as 0.3 weight percent (wt%; Stein 1990, Burdige 2006). Higher amounts of organic matter preservation require special environmental conditions, e.g. fast burial of organic matter by turbidites (Stein 1990). Burdige (2006) suggests that the organic carbon burial efficiency with respect to the original carbon rain rate to the sediment surface is on average ~10–20%.

The abundance of $BSiO_2$ in deep sea sediments is often interpreted in terms of productivity pattern of organisms such as diatoms (Koning *et al*. 1997). Biogenic silica or opal is a major component of the skeletal structure of diatoms, radiolaria, silicoflagellates and sponges (Koning *et al*. 2002). Among them, diatoms are the main producers of opal and strongly influence the cycling of silicon and carbon in the oceanic ecosystem (Cortese *et al*. 2004). Smear slides from ODP Site 1095 core sediments show that diatoms assemblages dominate (10–30%) and radiolarians and foraminifers are under-represented (Hillenbrand & Fütterer 2002). The accumulation of biogenic opal on the seafloor is controlled by bioproductivity, dissolution in the water column and diagenetic dissolution within the sediment. Opal preservation after burial is generally very poor. Schlüter (1990) determined that in the Weddell Sea, more than 90% of buried opal is dissolved in surficial sediments and released to the sediment-water interface. In general, increased sediment flux leads to faster burial and to better opal preservation (Ragueneau *et al*. 2000).

This study assumes that diatoms are the main carrier of the opal signal (Treguer *et al*. 1995), slope loading is dominated by terrigenous material from the shelf and hinterland during glacials, the quantity of diatom fossils settling down from the water column is continuous between two consecutive slope failures, and the laboratory determined leaching rate of biogenic silica from the

https://doi.org/10.1017/S0954102009990289 Published online by Cambridge University Press

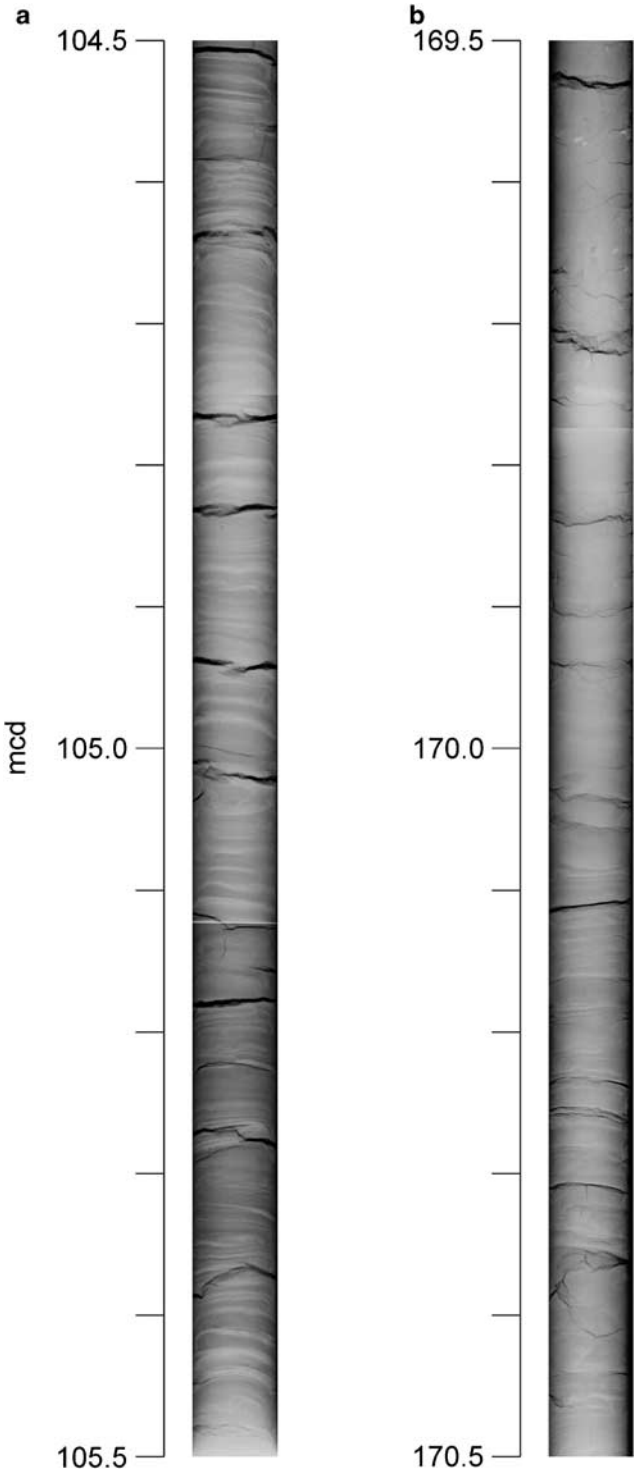


**Fig. 2.** Digital X-ray images from early Pliocene glacial intervals of ODP Site 1095 show the typical, fine laminated silt layer sequences. **a.** shows core section 1095B-3H6, 104.5–105.5 mcd from uppermost early Pliocene, and **b.** 1095B-10H5 to 10H6, 169.5–170.5 mcd from lowermost early Pliocene (see Fig. 3).

skeletal structure of diatoms is a function of their diagenetic and transport history.

*Regional settings*

This study is focused on the early Pliocene sedimentary record from Drift 7, which is one of the largest sediment mounds located south-west of the Antarctic Peninsula (Fig. 1). Its asymmetrical shape, with a short steep side facing south-east and a long, gently sloping side facing north-west, is similar in shape to the other sediment drifts in this area.

The distal part of Drift 7 was drilled by advanced piston corers and extended core barrels from Holes A and B at Site 1095 during ODP Leg 178 (ODP Leg 178 Shipboard Scientific Party 1999). The 561.78 m long composite record covers the late Miocene to the Holocene (~10 Ma).

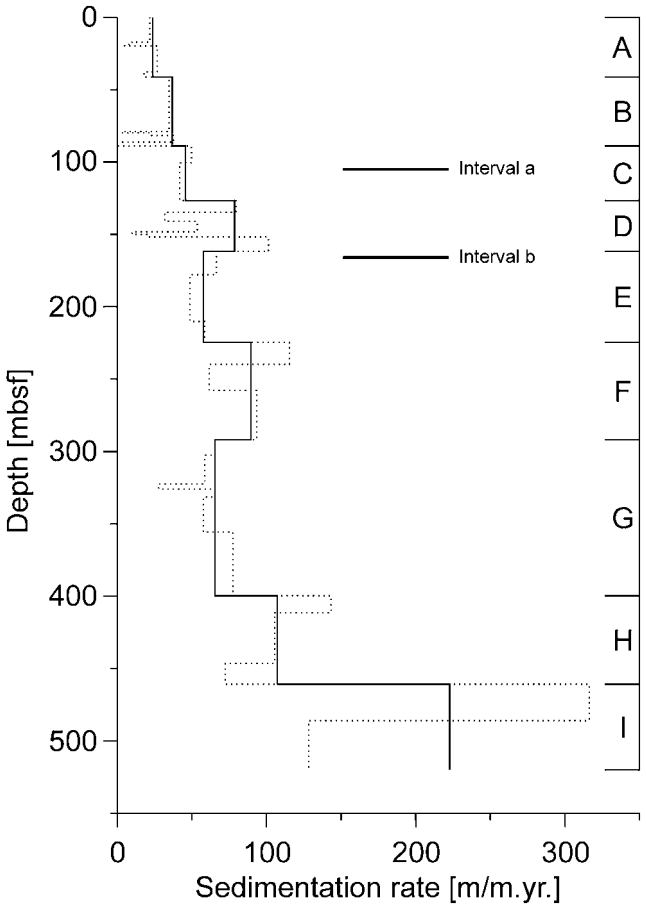


**Fig. 3.** Sedimentation rates (cm $kyr^{-1}$) for Site 1095 plotted vs depth. The dotted line shows the sedimentation rate based on a linear model from magnetostratigraphical-biochronological tie-points given in Acton *et al*. (2002) and Iwai *et al*. (2002). The solid line shows, for this study, a simplified linear sedimentation rate model with intervals A to I. For depth (meter below seafloor = mbsf) and age (Ma) tie-points see Table I. The bars show the depth position of the investigated core intervals (see Figs 2, 4 & 8).

https://doi.org/10.1017/S0954102009990289 Published online by Cambridge University Press

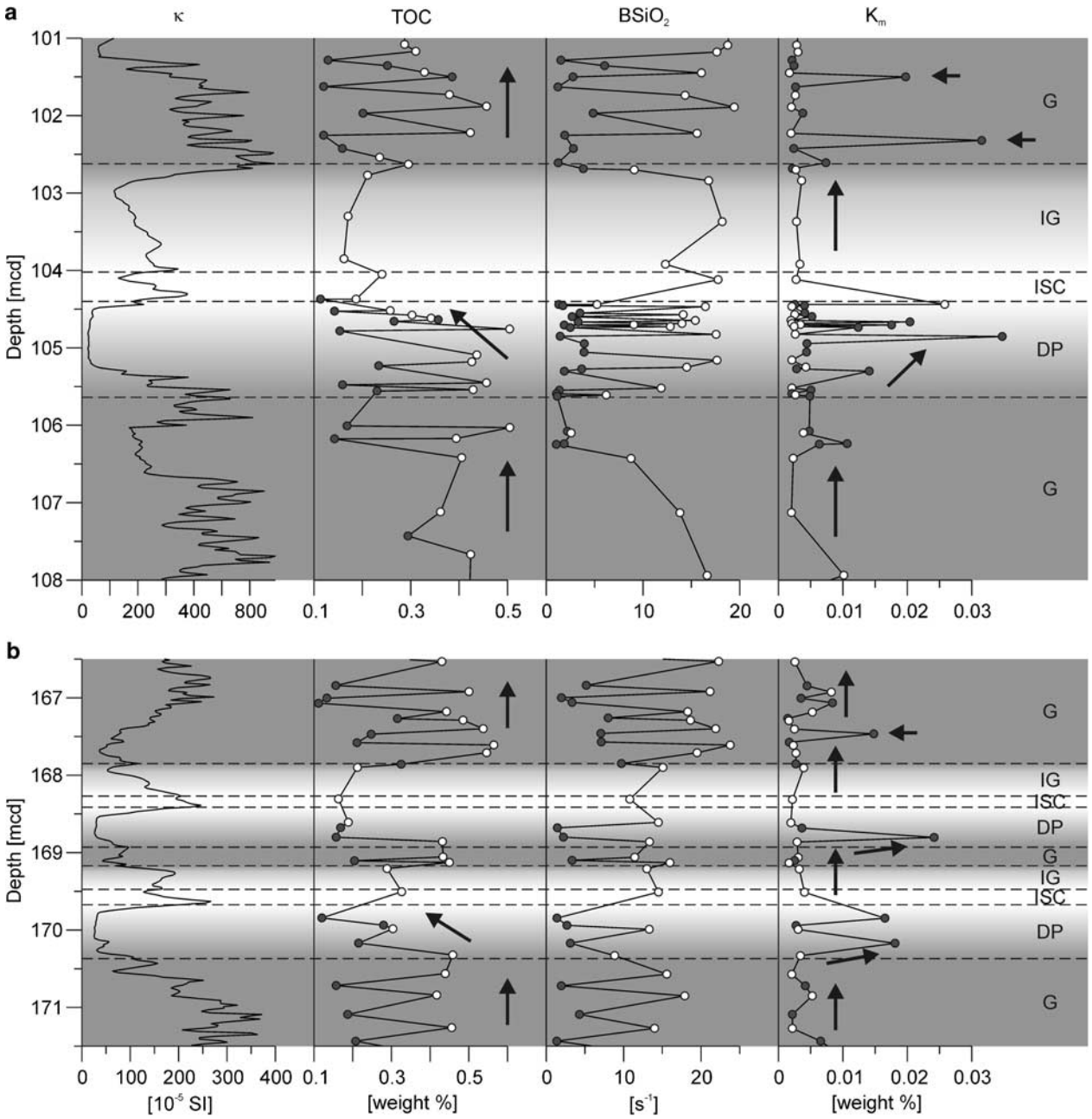


**Fig. 4.** Core intervals at **a.** 108.0–101.0 mcd, and **b.** 171.5–166.5 mcd of ODP Site 1095. The diagram shows magnetic susceptibility ($\kappa$), total organic carbon (TOC), biogenic silica content ($BSiO_2$) and the reaction rate constant of leached biogenic silica ($K_m$), in relation to glacial (G) and true interglacial (IG) stages, as well as deglaciation phases (DP) including the ice sheet collapse (ISC). The sediment samples were distinguished in samples from pure silt layers (filled circles) and sediments without silt layers (open circles). Characteristic gradients of TOC and $BSiO_2$ in relation to glacial stages are marked by arrows.

*Aims of this study*

Our study is aimed at quantifying the early Pliocene ice sheet dynamics via slope failure frequencies recorded in Antarctic Peninsula rise sediments. Crucial questions are a) how to determine the average time period between two consecutive turbidite events (turbidite frequency), and b) what other indicators can be used to support the derived model for palaeo ice sheet dynamics. The presented quantification approach of palaeo ice sheet dynamics is a contribution to the question c) how is the Pliocene Antarctic Peninsula ice sheet dynamic forced by Milankovich eccentricity (Grützner *et al*. 2003, 2005, Iorio *et al*. 2004, Hepp *et al*. 2006) or does it show autocyclic behaviour (Pudsey 2002)?

https://doi.org/10.1017/S0954102009990289 Published online by Cambridge University Press

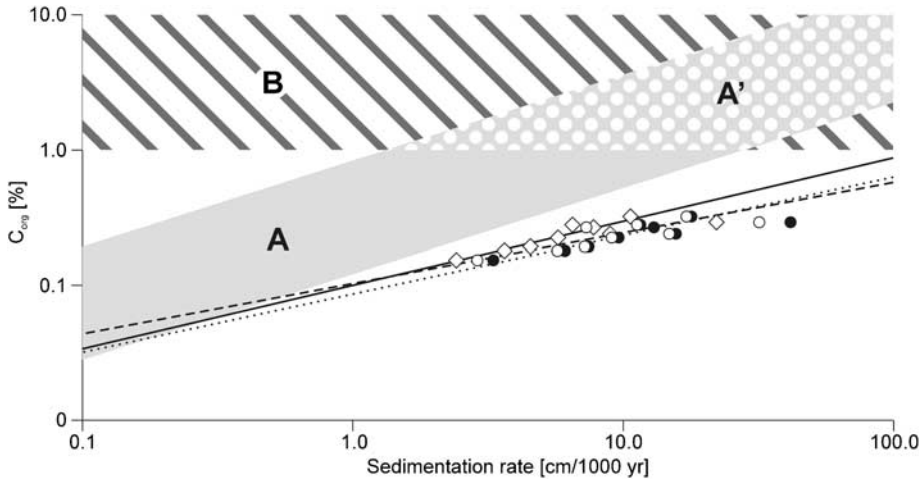


**Fig. 5.** Correlation between marine organic carbon and sedimentation rate (modified and simplified after Stein 1990). The model is based on data derived from Miocene to Pleistocene/Holocene sediment deposits in open marine (A) oxic, (A') upwelling high-productivity, and (B) anoxic environments. The symbols and power fit graphs show ODP Site 1095 data of compacted sediments (open rhombi, solid line) and decompacted sediments after Stein (1990) (Eq. (3); filled circles, dotted line) or after Terzaghi (Eq. (4); open circles, dashed line) respectively.

## Methods

X-ray images, sedimentary and geochemical analyses from two core intervals of ODP Site 1095 (a: 1095B-10H6 to 1095B-10H3, 171.5–166.5 mcd, lowermost early Pliocene; b: 1095B-4H2 to 1095B-3H4, 108.0–101.0 mcd, uppermost early Pliocene; mcd = revized metre composite depth after Barker 2002) were used to reconstruct turbidite recurrence frequencies in order to obtain a measure of the regional palaeo ice sheet dynamics.

### *Measurements*

Digital X-ray images (Fig. 2) were made from selected core sections at the Red Cross Hospital, Bremen using 'Fluorospot compact' radiography equipment. The dimension of the detector (measuring 40 to 80 cm) determines the size of the single X-ray image. Four overlapping images were produced to cover a 1.5 m core section. Ray penetration of 66 kV and an exposure time of 7.1 mA $s^{-1}$ were used. The high-resolution images were used to detect and map single silt layers, some of them with distinguishable Bouma sequences. Many of the mapped laminae with a total thickness less than $< 1$ mm have not been detected before from core images or visual descriptions. A definition of how to best define glacial-interglacial boundaries is given in Hepp *et al*. (2006).

The sedimentation rate (Fig. 3) is based on a magnetostratigraphical-biochronological age model given in Acton *et al*. (2002) and Iwai *et al*. (2002; dotted line). The black line shows a simplified linear sedimentation rate model.

Figure 4 shows parameter of magnetic susceptibility (κ), total organic carbon content (TOC), $BSiO_2$ and the reaction rate constant of leached biogenic silica ($K_m$) from two core intervals, 171.5–166.5 and 108.0–101.0 mcd, of ODP Site 1095 in relation to glacial and interglacial stages proposed by Hepp *et al*. (2006). Magnetic susceptibility (κ) data were obtained during ODP Leg 178 using the shipboard whole-core multisensor track logger (ODP Leg 178 Shipboard Scientific Party 1999). This fast, high-resolution measuring method is used here to distinguish glacial from deglaciation, ice sheet break down and interglacial intervals (see Hepp *et al*. 2006). The total organic carbon content (TOC) was measured by LECO on 55 samples. Left over material from the same samples was used to determine the biogenic silica content. The homogenized dry bulk samples were analysed using an automated leaching technique after Müller & Schneider (1993) and $K_m$ was calculated using a leaching model after Koning *et al*. (2002, Model 4). The TOC, $BSiO_2$ and $K_m$ measurements were distinguished in sediment samples from pure silt layers (Fig. 4, filled circles) and sediments without silt layers (fine fraction $< 63$ μm; Fig. 4, open circles).

### *Relationship of organic carbon and sedimentation rate*

In order to determine the average period between two consecutive turbidite events preserved in the silt layer record, glacial-interglacial sedimentation rates were derived from a positive long-term correlation of sedimentation rate and marine organic carbon content.

Stein (1990) showed that a positive correlation between organic carbon content and sedimentation rate exists (Fig. 5A and A'), since high sedimentation rates favour the preservation of organic matter by reducing the retention time in the shallow subsurface zone of bioturbation and oxic decomposition. Under anoxic deep bottom water conditions (Fig. 5B) he recognized no positive correlation between organic carbon and sedimentation rate. According to Stein (1990), the relationship between marine organic carbon ($C_{org}$) and sedimentation rate ($\omega$, cm $kyr^{-1}$) in recent sediments can be expressed as a log-linear function:

$$C_{org} = a\omega^b \tag{1}$$

or

$$\omega = \left(\frac{C_{org}}{a}\right)^{\frac{1}{b}} \tag{2}$$

https://doi.org/10.1017/S0954102009990289 Published online by Cambridge University Press

**Table I.** Simplified sedimentation rate model (see Fig. 3) computed for compacted and decompacted Eqs (3) & (4) sediments.

| Interval (Fig. 3) | Depth (mbsf) Top | Depth (mbsf) Bottom | Age (Ma) Top | Age (Ma) Bottom | $C_{org}$ (wt%) Mean average | Sedimentation rate (cm kyr$^{-1}$) Compacted | Decompacted Eq. (3) | Decompacted Eq. (4) |
|---|---|---|---|---|---|---|---|---|
| A | 0.00 | 41.29 | 0 | 1.95 | 0.15 | 2.43 | 3.32 | 2.90 |
| B | 41.29 | 88.68 | 1.95 | 3.33 | 0.18 | 3.66 | 6.11 | 5.74 |
| C | 88.68 | 126.20 | 3.33 | 4.18 | 0.19 | 4.56 | 7.48 | 7.24 |
| D | 126.20 | 161.31 | 4.18 | 4.98 | 0.27 | 7.81 | 13.05 | 7.33 |
| E | 161.31 | 224.30 | 4.98 | 6.137 | 0.22 | 5.77 | 9.66 | 9.11 |
| F | 224.30 | 292.04 | 6.137 | 6.935 | 0.24 | 8.98 | 15.73 | 14.87 |
| G | 292.04 | 399.86 | 6.935 | 8.635 | 0.28 | 6.52 | 11.62 | 11.30 |
| H | 399.86 | 460.87 | 8.635 | 9.23 | 0.32 | 10.69 | 17.96 | 17.22 |
| I | 460.87 | 520.50 | 9.23 | 9.58 | 0.29 | 22.24 | 41.77 | 32.00 |
| Mean average | | | | | 0.24 | 8.07 | 14.08 | 11.97 |

where the factor $a$ is 0.36 and the slope $b$ is 0.64 according to Stein's (1990) dataset.

To apply these functions to the relationship between preserved marine organic carbon and sedimentation rate of Pliocene sediments it is necessary to correct the apparent sedimentation rate by a decompaction factor ($DF$). Stein (1990) proposed the following relationship for the decompacted sedimentation rate ($\omega_0$, cm kyr$^{-1}$):

$$\omega_0 = \omega \cdot DF = \omega \cdot \frac{100 - \phi}{100 - \phi_0} \quad (3)$$

where $\Phi$ is the mean porosity of the Pleistocene samples in percent and $\Phi_0$ is the porosity of the freshly deposited sediment in the same depositional environment. In this

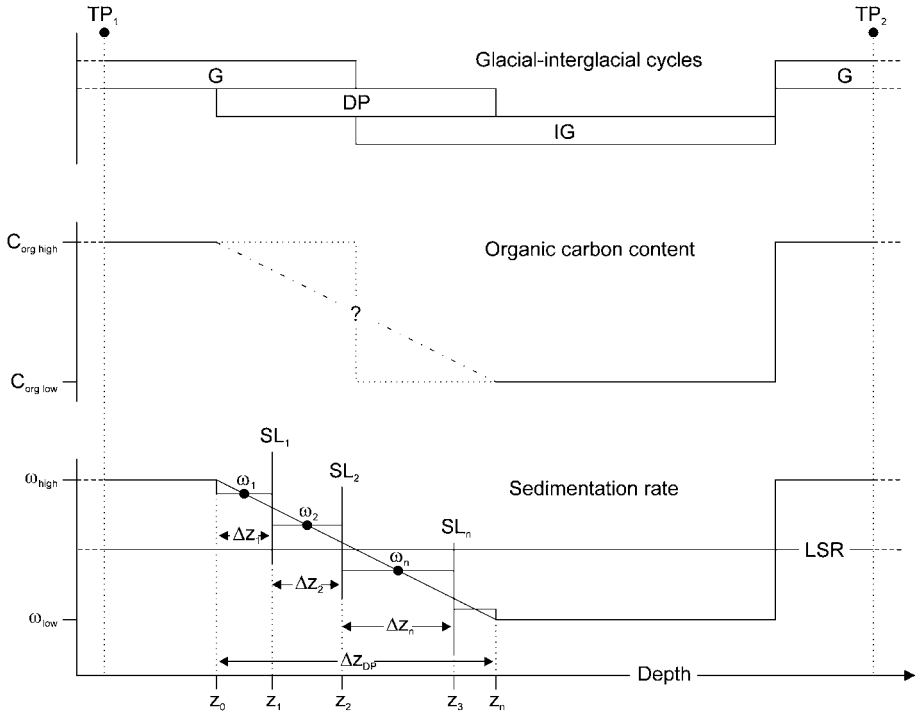


**Fig. 6.** Schematic diagram of the relationship between glacial-interglacial cycles, changes in the organic carbon content and changes in the sedimentation rate comprising following findings and boundary conditions: 1) The duration of glacial (G) and interglacial (IG) intervals is similar and the deglaciation phase (DP) spans equally both intervals, 2) The mean marine organic carbon content ($C_{org}$) correlates positively with the mean sedimentation rate (ω). Both, marine organic carbon contents and sedimentation rate are high in glacials, they decrease during deglaciation phase (glacial to interglacial transition), then achieve a lower level in the upper part of the interglacial and jump again to a high at the interglacial-glacial transition, 3) The linear sedimentation rate (LSR) based on a magnetostratigraphic-biochronologic age model given in Acton *et al*. (2002) and Iwai *et al*. (2002) and was computed using the tie-points $TP_1$ and $TP_2$, 4) For the deglaciation phase we calculated the duration and the relative timing of each silt layer (SL) depositions ($z_n$) on the basis of the length of the deglaciation phase ($z_{DP}$) and the sedimentation rates ($\omega_n$) coaxial between two adjacent silt layers ($\Delta z_n$) using the function given in Eq. (6). Results are given in Table II.

https://doi.org/10.1017/S0954102009990289 Published online by Cambridge University Press

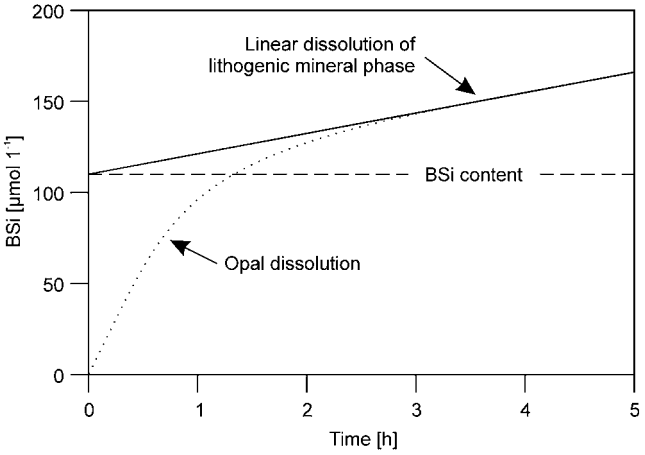


**Fig. 7.** Schematic sketch of an opal (BSi) dissolution curve (dotted line). The $SiO_2$ contribution of the lithogenic mineral phase can be extracted by a backward extrapolation of the linear fit of the dissolution curve. The corrected BSi content is retrieved from the fit curve at time zero (modified from Koning *et al*. 2002).

study, the porosity of near surface sediments of ODP Site 1095 was $\Phi_0 = 75\%$. For comparison, the average porosity for the Pliocene section is 59%.

A second approach to calculate decompacted sedimentation rates is based on Terzaghi's one dimensional consolidation theory (Azizi 2000, p. 170, eq. 4.1), restores the original sedimentation rates and is based on the volume independent void ratios:

$$\omega_0 = \frac{\Delta z_{\text{int}} + dh}{\Delta t_{\text{int}}} = \frac{\Delta z_{\text{int}} + \frac{\Delta z_{\text{int}} \cdot (e_0 - e)}{1 + e_0 - (e_0 - e)}}{\Delta t_{\text{int}}} = \frac{\Delta z_{\text{int}} + \Delta z_{\text{int}} \cdot e_0}{\Delta t_{\text{int}} + \Delta t_{\text{int}} \cdot e} \quad (4)$$

where $dh$ is the height loss by compaction, $\Delta z_{int}$ is the compacted interval length and $\Delta t_{int}$ is the time of deposition of each interval; $e_0$–$e$ is the difference between the initial and the measured void ratio of the compacted sediment as retrieved from the cores.

*Mean duration of glacials and interglacials in relation to the deglaciation phase*

On the basis of the mean average organic carbon content of each core interval from a composite splice of ODP Site 1095, the long-term correlation (9.8 Ma) between organic carbon and the compacted and decompacted sedimentation rate was calculated using Eqs (3) & (4), respectively. The data is plotted to a log-log scale and fitted by a power function (Fig. 5). The decompacted sedimentation rate is based on a simplified model (Fig. 3, solid line) of the linear sedimentation rate from magnetostratigraphical-biochronological age tie-points given in Acton *et al*. (2002) and Iwai *et al*. (2002; Fig. 3, dotted line). The data are given in Table I.

The compacted and decompacted linear sedimentation rates were used to calculate the mean duration of glacials ($\Delta t_{avG}$) between neighbouring magnetostratigraphical-biochronological age tie-points in the time interval from 5.98 to 3.22 Ma (latest Miocene to mid–late Pliocene):

$$\Delta t_{avG} = \frac{\Delta z_{avG} \cdot \Delta t_{avGIG}}{\Delta z_{avG} + \Delta z_{avIG} \cdot \omega_{av\,ratio}} \quad (5)$$

where $\Delta z_{avG}$ and $\Delta z_{avIG}$ are the mean average length of glacials and interglacials respectively, $\Delta t_{avGIG}$ is the mean average period defined by the age tie-points 5.98 Ma and 3.22 Ma (= 2.67 Ma) divided by the number of identified glacial-interglacial cycles (= 22). The linear sedimentation rate ratio ($\omega_{av\ ratio}$) between glacials and interglacials is calculated from the compacted mean average linear sedimentation rate and decompacted linear sedimentation rates using Eqs (3) & (4).

To further refine the mean duration of glacials and interglacials, a model of three main sedimentary stages within a glacial-interglacial cycle was used (Hepp *et al*. 2006): a) Full glacial (G), b) deglaciation phase (DP) including the ice sheet collapse (ISC), and c) ice sheet growth phase, here referred as true interglacial (IG). An example for this model is shown in Fig. 4.

The refinement is necessary since the deglaciation phase was previously unconsidered. This could lead to an inaccurate estimate of the initial, mean average glacial-interglacial interval length and period respectively, because the boundaries of the deglaciation phase are only definable with

**Table II.** Computation of the mean average period of glacials ($\Delta t_{zavG + DP/2}$) and interglacials ($\Delta t_{zavIG + DP/2}$), each include half of a deglaciation phase, between the magnetostratigraphic-biochronologic age tie-points 5.98 and 3.22 Ma. Given are the results from different models on basis of linear sedimentation rates (see Table I) from (a) compacted sediments and decompaction models after (b) Stein (1990; see Eq. (3)), and (3) Terzaghi (see Eq. (4)). These values were used for Eq. (5).

| Model | $\Delta z_{avG + DP/2}$ (cm) | $\Delta z_{avIG + DP/2}$ (cm) | $\Delta TOC_{avG}$ (wt%) | $\Delta TOC_{avIG}$ (wt%) | $\Delta_{avG}$ (cm kyr$^{-1}$) | $\Delta_{avIG}$ (cm kyr$^{-1}$) | $\Delta_{avG/IG}$ ratio | $\Delta t_{avG}$ (kyr) | $\Delta t_{avIG}$ (kyr) |
|---|---|---|---|---|---|---|---|---|---|
| 1 | 252.700 | 155.167 | 0.324 | 0.296 | 12.383 | 10.636 | 1.164 | 71.068 | 50.295 |
| 2 | 417.323 | 257.014 | 0.324 | 0.296 | 21.801 | 17.644 | 1.236 | 65.264 | 56.100 |
| 3 | 400.202 | 245.561 | 0.324 | 0.296 | 21.614 | 16.930 | 1.277 | 63.983 | 57.381 |

https://doi.org/10.1017/S0954102009990289 Published online by Cambridge University Press

a complex multi-parameter approach (Hepp *et al*. 2006). Deglaciation phases are influenced by a decline in glacial silt deposition and an increase in interglacial organic input.

Another problem with using the positive correlation of sedimentation rate and marine organic carbon content arises from the significant diagenetic influence on the organic carbon preservation during the deglaciation phase reported by Hepp *et al*. (2006). The model of organic carbon-sedimentation rate correlation is not suitable to calculate the duration of the deglaciation phase. To limit the uncertainties introduced by the 'deglaciation phase problem' a linear decrease of the sedimentation rate from a higher glacial to a lower interglacial level was assumed. A simple glacial-interglacial model with a deglaciation phase spanning equal parts of both depths intervals was used. The duration of the deglaciation phase and the relative timing $t(z)$ of each silt layer (SL) depositions ($z$) was calculated on the basis of the length in decompacted core meters of the deglaciation phase $z_{DP}$ and glacial and interglacial sedimentation rates $\omega_G$, $\omega_{IG}$ using the function:

$$t(z) = \frac{1}{2} \cdot \frac{\omega_{IG} - \omega_G}{z_{DP}} \cdot z^2 + \omega_G \cdot z \qquad (6)$$

The model is sketched in Fig. 6 and the results are given in Table II.

### *Leaching rate of biogenic silica* (*opal-A*)

In order to support the derived turbidite frequency data we also looked at opal dissolution parameters as an additional approach to quantify the retention time between two consecutive slope failures. The reaction rate constant from automated leaching methods of biogenic silica, in the following called leaching rate, was used as an indicator for the preservation state of diatom frustules. Exposure times and preservation stage may vary depending on the relative time of the frustules spend for vertical settling through the water column, burial in the sediment or during transport and depositional processes on the continental shelf, slope and rise, respectively.

Most of the reactive silica in marine sediments has a biogenic origin (Koning *et al*. 2002). Since the Si-dissolution of $BSiO_2$ occurs independently from dissolution of the lithogenic phase from clay minerals (DeMaster 2002) it is necessary to distinguish between dissolving biogenic silica and silica from clay minerals. Si-dissolution from clay minerals has a linear and much slower reaction rate than of $BSiO_2$. Corrections for $BSiO_2$ from the lithogenic mineral phase can be achieved by extrapolation of the linear dissolution trend and subtraction from the measured total dissolved $BSiO_2$ (Fig. 7).

Müller & Schneider (1993) proposed an automated alkaline leaching method to determine the biogenic silica content in surface sediments and to discriminate between

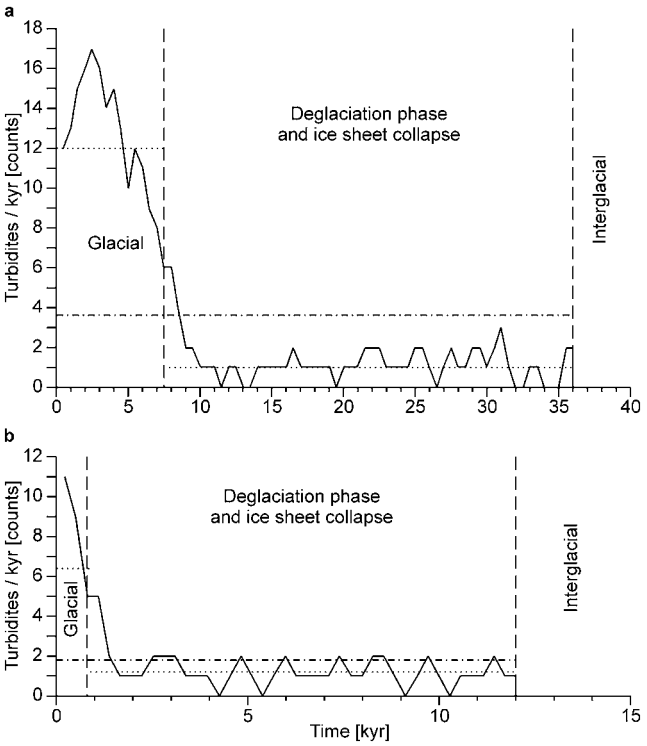


**Fig. 8.** Early Pliocene turbidite frequency for ODP 1095 core section between **a.** 105.64–104.02 mcd, and **b.** 168.93–168.27 mcd. The diagram shows a decrease in turbidite frequency during the deglaciation and the ice sheet collapse phase. The number of turbidites per 1 kyr was plotted on the ordinate. The dotted line shows the mean average turbidite ratio for the glacial interval and the deglaciation phase respectively. The chain line shows the mean average of the total turbidite interval.

**Table III.** Conceptual model for the interplay of retention time of diatom skeletons on the shelf and slope, transport by downslope mass wasting processes, burial rate on the drift and the effects of these three laboratory opal leaching rate under different glacial-interglacial conditions in the Pliocene. A combination of prolonged retention times, fragmentation and relatively fast burial leads to increased laboratory leaching rates.

| Interval | Shelf and slope | | Downslope processes | Drift | Laboratory measurement |
|---|---|---|---|---|---|
| | Retention time | Opal dissolution | Mechanical fragmentation | Burial rate | Leaching rate |
| Full glacial | short | low | high | high | low |
| Deglaciation phase | increase | increase | high | decrease | high |
| Interglacial | long | high | none | low | low |
| Onset of glacial | long | high | high | high | high |

https://doi.org/10.1017/S0954102009990289 Published online by Cambridge University Press

leached silica from the biogenic fraction and the lithogenic fraction. The digital data of the leaching curves were run through a fitting procedure after Koning *et al*. (2002, Model 4) to obtain a measure of the biogenic silica reactivity via the reaction rate constant ($K_m$):

$$K_m \frac{v}{\alpha([Si_{extr}])^{1/v}} \quad (7)$$

where $Si_{extr}$ is the initial extractable Si ($\mu m\, l^{-1}$), $\alpha$ measures the average lifetime of the extractable components in the mixture and $v$ is a non-dimensional parameter.

## Results

The early Pliocene turbidite frequency for Drift 7 was determined via the calculation of the glacial-interglacial duration, which is based on the organic carbon correlated sedimentation rate model (Fig. 8, Tables I & II). The results from leaching rate measurements of biogenic silica show the interaction of retention time, transport mechanisms and burial rate during glacial-interglacial cycles (Table III).

### *Positive correlation of organic carbon and sedimentation rate*

The mean organic carbon content (0.24 wt%; see Table I) from ODP Site 1095 samples is typical for open ocean deep sea sediments. The compacted and decompacted sediment data (Fig. 5) show that a positive correlation exists between organic carbon content and sedimentation rate. The power fit of the data in a log-log distribution can be described with the function given in Eqs (1) & (2), where for compacted sediments the constant $a$ is 0.9 and $b$ is 0.47, and for decompaction using Eq. (3) or (4) $a$ is ~0.1 and $b$ is 0.43 or 0.37 respectively.

### *Compaction-decompaction models*

The calculated glacial-interglacial duration (Table II, $\Delta t_{avG}$ and $\Delta t_{avIG}$) show differences of up to 7 kyr between the compaction-decompaction models. The glacial-interglacial sedimentation rate ratio of the two models using decompacted sedimentation rates (Eqs (3) & (4); Table II) is very similar. In the following calculation, Model 3, based on decompaction method after Terzaghi, was used since the void ratio conserves the particle mass and is therefore more appropriate to estimate glacial to interglacial material property changes. The derived sedimentation rate ratio of 1.28 (Table II, Model 3) matches the mean average glacial–interglacial thickness ratio of 1.27 suggested in an earlier paper of Hepp *et al*. (2006). The application of Model 3 (Table II), leads to reasonable mean average glacial periods of 63.98 kyr and mean average interglacial periods of 57.38 kyr. The slight asymmetry toward glacial periods is explained by the ice proximity of the core location.

### *Turbidite frequency*

To estimate the frequency distribution of silt layers from ODP Site 1095 cores, the results from Model 3 were integrated with the X-ray derived turbidite counts. The resulting turbidite frequency model (Fig. 6) is based on the following axioms:

a. The glacial-interglacial periodicity is strongly controlled by Milankovitch cycles (Grützner *et al*. 2003, Iorio *et al*. 2004) and the average proportion of glacial to interglacial time periods follow Model 3.

b. The ice sheet evolution on the shelf is closely coupled to the sedimentary depositional patterns on the drift and changes in the sedimentary supply reflect regional ice sheet advances, retreats and collapses (Hepp *et al*. 2006, Bart *et al*. 2007).

c. The sediments of glacials are strongly dominated by terrigenous supply (turbidites) with high sedimentation rates. The sediments of interglacials are dominated by pelagic settling of biogenic material and terrigenous material derived from ice rafted debris and wind transport with lower sedimentation rates (Hepp *et al*. 2006).

d. The linear sedimentation rate computed from magnetostratigraphical-biochronological tie-points given in Acton *et al*. (2002) and Iwai *et al*. (2002) corresponds to the mean average sedimentation rate from all glacials and interglacials of the studied Pliocene core section.

e. Excellent preservation of turbidite-derived silt layers exist on the distal part of the drift at ODP site 1095.

On the basis of this conceptual model, the frequency distribution of silt layers for two early Pliocene glacial to interglacial transitions (168.93 to 168.27 and 105.64 to 104.02 mcd) from core sections of ODP Site 1095 was calculated. For these two sections, the average turbidite re-occurrence is ~375 yrs. A moving average with a 1 kyr window for the section between 105.64 to 104.02 mcd (Fig. 8a) and a 0.5 kyr window for the section between 168.93 to 168.27 mcd (Fig. 8b) was used to determine frequencies from silt layer reoccurrences.

The resulting graphs (Fig. 8) show a decrease in turbidite frequency during the deglaciation phase and the ISC which correlates to a time interval of reduced terrigenous sedimentation supply as proposed by Hepp *et al*. (2006). Figure 8 shows the mean average number of turbidites per 1 kyr is ~6.6 turbidites/kyr for glacial intervals and ~2.8 turbidites/kyr for the deglaciation phase.

### *Retention time between two consecutive slope failures*

In Fig. 4, the total organic carbon (TOC), biogenic opal ($BSiO_2$) content, and the opal leaching rate ($K_m$) of two early Pliocene core sections (171.5–166.5 and 108–101 mcd) are

https://doi.org/10.1017/S0954102009990289 Published online by Cambridge University Press

shown. The bulk magnetic susceptibility (κ) aids in differentiating glacial and interglacial stages. All opal data are measured on the fine fraction (< 63 μm) and distinguishes data from sediment samples with silt layers (solid circles) and without silt layers (open circles).

The $BSiO_2$ data show that the general opal content in interglacials (mean average of sediments without silt layers is 15.90 wt%) is slightly higher than in glacials (mean average of silt layers is 2.16 and of sediments without silt layers is 11.35 wt%). Comparing the opal contents with regard to host sediment grain size, we observe a significantly higher opal content in samples without silt layers (2.57–18.19 wt%) than in silt layer samples (1.06–3.93 wt%).

The leaching rate of opal ($K_m$) is independent of the total opal concentration in the sample and shows no significant variances between glacial to interglacial stages. Focused on deglaciation phases (Fig. 4, DP) and the lower part of glacials (Fig. 4, G) the leaching rate from silt layer samples (mean average 0.0089 $s^{-1}$) diverges from the overall low background rates and sediment (mean average 0.0027 $s^{-1}$). In Fig. 4a, a gradual increase in leaching rate during the deglaciation phase is observed with the exception of the last three samples with low values, which correlate negatively with the gradual decrease in silt layer frequency (Fig. 8a). The beginning of glacials is characterized by distinct peaks in leaching rate.

## Discussion

### *Close relationship of ice sheet advances, slope loading and frequent slope failure*

In the absence of major fluvial systems, the ice sheet is the main driving force behind erosion, transport and deposition of terrigenous material from the continental shelf to the deep sea sediment drifts. Ice thickness, flow velocity and frequency of advances to the shelf edge determine the amount of material transported to the continental slope. The slope angle is another important component determining transportation rate to the rise. The slope angle is determined by the type of transported material (e.g. coarse material from an erosive glacial advance leads to a steep slope; (Rebesco *et al*. 1996).

The current West Antarctic ice sheet is assumed to have the capability of rapidly shrinking, because the grounding line between the continental ice sheet and the floating ice shelves is mostly far below sea level and thus unstable (Bentley 1998, Raymond 2002). In a recent study of ice sheet dynamics controlled by sedimentary processes along the Antarctic Peninsula continental margin, Hepp *et al*. (2006) proposed a highly dynamic early Pliocene ice sheet with abrupt changes in lithology at interglacial to glacial transitions. A conspicuous feature is the abrupt cessation of ice rafted debris (IRD) input and the synchronous onset of frequent silt layer deposition. The factors controlling the rapid interglacial to glacial transition are not completely understood, but rapid ice re-advances to the shelf edge may point towards an ice sheet which does not fully retreat to the shoreline during interglacials.

In view of the glacial-interglacial cyclicity in the Pliocene, the turbidite depositional regime at ODP Site 1095 shows a consistent pattern in silt layer distribution and frequency (Hepp *et al*. 2006). In the early Pliocene the silt layers are closely spaced and the reoccurrence frequency is continuously high in glacials. The frequency distribution of silt layers is interpreted to reflect short and rapid but continuing ice advances every ~375 yrs. This full glacial depositional pattern is followed by a gradual decrease in silt layer frequency during the deglaciation phase. The ice sheet collapse and the ice sheet growth phases within the interglacial intervals contain no silt layers.

The reaction rate constant ($K_m$), determined from the $BSiO_2$ leaching measurements, was used as an indicator of the diagenetic and transport history of the diatom frustules. The rate constant describes the dissolving rate of opal and depends on the texture and preservation stage of diatom frustules and the deposition mode. Large diatom frustules with complex morphology have a more dissolvable surface than smaller and simpler frustule structures (McManus *et al*. 1995, Rabouille *et al*. 1997). A larger surface of fragmented diatom frustules dissolves faster than intact skeletons. Van der Weijden & van der Weijden (2002) demonstrated the dependency of opal dissolution rate on the reactivity of the opal. They showed that both linked processes decrease with increasing burial depth of the biogenic silica matter. Rapid burial under overall high sedimentation rate (e.g. turbidite events) reduces the reaction time and increases the preservation of reactive opal in the sedimentary record, whereas, under low sedimentation rates, long exposure at the sediment-water interface fosters the dissolution of reactive opal. This leads to diatom remnants in the sediment record that show slow reaction rate constants in laboratory leaching tests. Thus, the reaction rate constant ($K_m$) is an indicator for the exposure time or post depositional transport process of biogenic opal from the continental shelf or slope to the drift recorder.

The results from this study suggest that the combined effects of retention time, transport mechanisms and burial rate are sufficient to explain the observed glacial-interglacial patterns in the opal leaching rate constant. High leaching rates result from a combination of long retention times on the shelf or slope, subsequent mechanical size reduction during reworking of the already weakened frustules during turbiditiy transport, and rapid burial. Low leaching rates indicate either short retention times in combination with rapid burial or long retention times in combination with slow burial. An overview of the transport and deposition effects on laboratory opal leaching rate under different glacial-interglacial conditions is given in Table III.

https://doi.org/10.1017/S0954102009990289 Published online by Cambridge University Press

Characteristic gradients of TOC and $BSiO_2$ in relation to glacial stages are marked by arrows in Fig. 4 and will be discussed in the following: low opal leaching rates during glacials point to a dynamic ice sheet during warm Pliocene ice sheet conditions. Periodically advancing and retreating ice streams discharge large amounts of terrigenous material to the continental slope triggering frequent slope failures (7–12 events per kyr; Fig. 8). Contained in every mass wasting are diatom skeletons deposited on the slope and shelf between two consecutive turbidite events. Short retention times on the shelf or slope prevents a dissolution induced weakening of the frustules. Stable frustules in turn have a higher probability to resist mechanical downsizing during turbiditic reworking. Fast deposition on the drift leading subsequently to small dissolution rates in the laboratory. During deglaciation a decrease in turbidite frequency and prolonged exposure times lead to weaker frustules that experience more mechanical downsizing during turbiditic reworking. Together with the fast deposition and burial, reactive opal gets preserved on the drift. The last three turbidites of the deglaciation phase, however, show lower leaching rate constants. These low leaching rates indicate a burial rate below a critical threshold that would be necessary to preserve the reactive opal fraction. In contrast, the interglacials show that long retention times, no turbiditic reworking and low hemipelagic burial rates allow an effective removal of reactive silica. A few peaks in the leaching rate from silt layer samples during the onset of glacials supports our conceptual model (see Table III for details).

### *Orbital periodicity in the early Pliocene*

The investigated area is sensitive to changes in ice sheet volume in West Antarctica and hence allows regional insights. Barker & Camerlenghi (2002) showed that the release of glacial sediments is cyclic and orbitally controlled. From early to late Pliocene intervals of Site 1095 cores Iorio *et al*. (2004) compiled strong short eccentricity periodicities (~95–125 kyr). This finding corresponds to our results with periodicities at ~120 kyr. For Pliocene time sections of ODP Site 1095 cores, a forcing by obliquity periodicities at about 50–60 kyr were reported in different studies: Wavelet analyses of petrophysical measurements show periodicities at 56 kyr and 87 kyr (Lauer-Leredde *et al*. 2002), and power spectra analyses show periodicities at 63 kyr (Pudsey 2002) and at 50 kyr and 64 kyr (Iorio *et al*. 2004) in magnetic susceptibility and chromaticity parameter a*. Our study indicates that these periodicities are most likely to respond to the glacial or interglacial half-cycles at 61.59 kyr and 59.77 kyr. Thus for the early Pliocene and the regional ice sheet behaviour we suggest that these periodicities do not reflect the combined effect of precession and obliquity periodicities as predicted by Berger (1977), Iorio *et al*. (2004) and Grützner *et al*. (2005).

## Conclusion

This study was intended to improve the understanding of the interaction of ice sheet dynamics, slope loading slope failure as reflected in turbidity sediment depositions along the Pacific continental margin of the Antarctic Peninsula during the early Pliocene. We have linked the turbidite frequency and the average time period between two consecutive turbidite events to reaction rate constant measurements on reworked biogenic opal to derive an indirect measure of the slope retention times for two core intervals of ODP Site 1095.

By using the long-term sedimentation rate dependency of the marine carbon burial efficiency in Antarctic drift sediments, it was possible to calculate a ratio of glacial to interglacial sedimentation rates for the Pliocene. Pliocene glacial-interglacial periodicities were determined by using sparse magneto and biostratigraphical tie points and counts of glacial and interglacial intervals. Together with the decompacted average length of glacial and interglacials, a set of linear equations for the glacial and interglacials half-periods and thus absolute half-cycle sedimentation rates were calculated. Decompaction following Terzaghi's one dimensional consolidation theory and a glacial-interglacial ratio of 1:1 for the deglaciation phase worked best in minimising uncertainties in our calculations. The deglaciation phase required a special adjustment because a diagenetic imprint on the organic carbon preservation prevents the organic carbon sedimentation rate correlation approach for the calculation of the duration of the deglaciation phase. Even for this shelf-proximal site the glacial and interglacial half-periods have on average equal durations of 63.98 kyr and 57.38 kyr, respectively. Derived average glacial turbidite recurrences of ~375 yr are interpreted as short and rapid ice sheet advances at relatively regular intervals resulting in continuous and periodic slope failures in the late Miocene/early Pliocene warm phase.

Frequent turbidite recurrences imply short retention times between slope loading and slope failure. This finding is supported by low reaction rate constants of opal leaching experiments during early Pliocene glacials. A significant increase of the leaching rate from silt layer samples is associated with a decrease of the turbidite frequency during the deglaciation phase. The complex opal dissolution behaviour observed in the laboratory is explained with a conceptual model of opal exposure, transport and burial. The findings from silt layer frequency distribution and biogenic silica leaching rates imply a close interaction between ice sheet dynamics, sediment discharge, slope loading and slope failure.

The ~120 kyr Pliocene glacial-interglacial periodicities correspond to data from wavelet and power spectra analyses from ODP Site 1095 on the Pacific continental rise of the Antarctic Peninsula. The previously predicted combined effect of precession and obliquity periodicity of

https://doi.org/10.1017/S0954102009990289 Published online by Cambridge University Press

~60 kyr from magnetic susceptibility data suggest to correspond rather to glacial or interglacial half-cycles respectively.

## Acknowledgements

Samples were provided by the Ocean Drilling Program (ODP). We thank the Bremen Core Repository (BCR) team for their kind support. The $BSiO_2$ measurements were carried out at the Alfred Wegener Institute of Polar and Marine Research (AWI) in Bremerhaven. The help of Dr Gerhard Kuhn und Rita Fröhlking during these measurements is greatly appreciated. We thank Jens Seeberg-Elverfeldt for his useful advice for the linear fitting of opal dissolution curves. Some $BSiO_2$ data from individual samples were part of a bachelor thesis by Sophie Fath prepared in our working group. Special acknowledgment goes to Stefan Kreiter (MARUM) for his help with the calculation of the turbidite frequencies. We thank Rüdiger Stein (AWI) for careful reading of our manuscript and we thank Diane Winter and Ellen Cowan for their reviews which improved our manuscript. This research was funded by the German Research Foundation (DFG project MO1059/1 and HE5377/1) and by the MARUM - Center for Marine Environmental Sciences, University of Bremen.

## References

Acton, G.D., Guyodo, Y. & Brachfeld, S.A. 2002. Magnetostratigraphy of sediment drifts on the continental rise of West Antarctica (ODP Leg 178, Sites 1095, 1096, and 1101). *In* Barker, P.F., Camerlenghi, A., Acton, G.D. & Ramsay, A.T.S., *eds*. *Proceedings of the Ocean Drilling Program, Scientific Results*, **178**, 1–61.

Anderson, J.B., Wellner, J.S., Lowe, A.L., Mosola, A.B. & Shipp, S.S. 2001. Footprint of the expanded West Antarctic ice sheet: ice stream history and behavior. *GSA Today*, **11**, 4–9.

Azizi, F. 2000. *Applied analyses in geotechnics*. London: Routledge, 254 pp.

Barker, P.F. 2002. Composite depths and spliced sections for Leg 178 Sites 1095 and 1096, Antarctic Peninsula continental rise. *In* Barker, P.F., Camerlenghi, A., Acton, G.D. & Ramsay, A.T.S., *eds*. *Proceedings of the Ocean Drilling Program, Scientific Results*, **178**, 1–15.

Barker, P.F. & Camerlenghi, A. 2002. Glacial history of the Antarctic Peninsula from Pacific margin sediments. *In* Barker, P.F., Camerlenghi, A., Acton, G.D. & Ramsay, A.T.S., *eds*. *Proceedings of the Ocean Drilling Program, Scientific Results*, **178**, 1–40.

Bart, P.J., Hillenbrand, C.-D., Ehrmann, W.U., Iwai, M., Winter, D. & Warny, S.A. 2007. Are Antarctic Peninsula Ice Sheet grounding events manifest in sedimentary cycles on the adjacent continental rise? *Marine Geology*, **236**, 1–13.

Bentley, C.R. 1998. Ice on the fast track. *Nature*, **394**, 21–22.

Berger, A.L. 1977. Support for the astronomical theory of climatic change. *Nature*, **269**, 44–45.

Burdige, D.J. 2006. *Geochemistry of marine sediments*. Princeton, NJ: Princeton University Press, 609 pp.

Cortese, G., Gersonde, R., Hillenbrand, C.-D. & Kuhn, G. 2004. Opal sedimentation shifts in the World Ocean over the last 15 Myr. *Earth and Planetary Science Letters*, **224**, 509–527.

DeMaster, D.J. 2002. The accumulation and cycling of biogenic silica in the Southern Ocean: Revisiting the marine silica budget. *Deep-Sea Research II*, **49**, 3155–3167.

Diviacco, P., Rebesco, M.A. & Camerlenghi, A. 2006. Late Pliocene mega debris flow deposit and related fluid escapes identified on the Antarctic Peninsula continental margin by seismic reflection data analysis. *Marine Geophysical Researches*, **27**, 109–128.

Dowdeswell, J.A., Ó Cofaigh, C. & Pudsey, C.J. 2004. Continental slope morphology and sedimentary processes at the mouth of an Antarctic palaeo-ice stream. *Marine Geology*, **204**, 203–214.

Elverhøi, A., Hooke, R.L. & Solheim, A. 1998. Late Cenozoic erosion and sediment yield from the Svalbard–Barents Sea region: implications for understanding erosion of glacierized basins. *Quaternary Science Reviews*, **17**, 209–241.

Grützner, J., Hillenbrand, C.-D. & Rebesco, M.A. 2005. Terrigenous flux and biogenic silica deposition at the Antarctic continental rise during the late Miocene to early Pliocene: implications for ice sheet stability and sea ice coverage. *Global and Planetary Change*, **45**, 131–149.

Grützner, J., Rebesco, M.A., Cooper, A.K., Forsberg, C.F., Kryc, K.A. & Wefer, G. 2003. Evidence for orbitally controlled size variations of the East Antarctic ice sheet during the late Miocene. *Geology*, **31**, 777–780.

Hepp, D.A., Mörz, T. & Grützner, J. 2006. Pliocene glacial cyclicity in a deep-sea sediment drift (Antarctic Peninsula Pacific Margin). *Palaeogeography, Palaeoclimatology, Palaeoecology*, **231**, 181–198.

Hillenbrand, C.-D. & Fütterer, D.K. 2002. Neogene to Quaternary deposition of opal on the continental rise west of the Antarctic Peninsula, ODP Leg 178, Sites 1095, 1096, and 1101. *In* Barker, P.F., Camerlenghi, A., Acton, G.D. & Ramsay, A.T.S., *eds*. *Proceedings of the Ocean Drilling Program, Scientific Results*, **178**, 1–33.

Iorio, M., Wolf-Welling, T.C.W. & Mörz, T. 2004. Antarctic sediment drift and Plio–Pleistocene orbital periodicities (ODP Sites 1095, 1096, and 1101). *In* D'Argenio, B., Fischer, A.G., Silva, I.P., Weissert, H. & Ferreri, V., *eds*. *Cyclostratigraphy: approaches and case histories*. Tulsa, OK: Society for Sedimentary Geology, 231–244.

Iwai, M., Acton, G.D., Lazarus, D.B., Osterman, L.E. & Williams, T. 2002. Magnetobiochronologic synthesis of ODP Leg 178 rise sediments from the Pacific sector of the Southern Ocean: Sites 1095, 1096, and 1101. *In* Barker, P.F., Camerlenghi, A., Acton, G.D. & Ramsay, A.T.S., *eds*. *Proceedings of the Ocean Drilling Program, Scientific Results*, **178**, 1–40.

Koning, E., Epping, E. & van Raaphorst, W. 2002. Determining biogenic silica in marine samples by tracking silicate and aluminium concentrations in alkaline leaching solutions. *Aquatic Geochemistry*, **8**, 37–67.

Koning, E., Brummer, G.-J., van Raaphorst, W., van Bennekom, J., Helder, W. & van Iperen, J. 1997. Settling, dissolution and burial of biogenic silica in the sediments off Somalia (northwestern Indian Ocean). *Deep-Sea Research II*, **44**, 1341–1360.

Lauer-Leredde, C., Briqueu, L. & Williams, T. 2002. A wavelet analysis of physical properties measured downhole and on core from Holes 1095B and 1096C (Antarctic Peninsula). *In* Barker, P.F., Camerlenghi, A., Acton, G.D. & Ramsay, A.T.S., *eds*. *Proceedings of the Ocean Drilling Program, Scientific Results*, **178**, 1–43.

Løseth, T.M. 1999. *Submarine massflow sedimentation: computer modelling and basin-fill stratigraphy*. Berlin: Springer, 156 pp.

Lucchi, R.G., Rebesco, M.A., Busetti, M., Caburlotto, A., Colizza, E. & Fontolan, G. 2002. Sedimentary processes and glacial cycles on the sediment drifts of the Antarctic Peninsula Pacific margin: preliminary results of SEDANO-II project. *New Zealand Journal of Geology and Geophysics*, **35**, 275–280.

McGinnis, J.P. & Hayes, D.E. 1995. The roles of downslope and along-slope depositional processes: southern Antarctic Peninsula continental rise. *Antarctic Research Series*, **68**, 141–156.

McManus, J., Hammond, D.E., Berelson, W.M., Kilgore, T.E., Demaster, D.J., Ragueneau, O.G. & Collier, R.W. 1995. Early diagenesis of biogenic opal: dissolution rates, kinetics, and paleoceanographic implications. *Deep-Sea Research II*, **42**, 871–903.

Mörz, T. 2002. *From the inner shelf to the deep sea: depositional environments on the West Antarctic Peninsula margin: a sedimentological and seismostratigraphic study* (*ODP Leg 178*). PhD thesis, Alfred Wegener Institut für Polar- und Meeresforschung, Bremerhaven, 236 pp.

Müller, P.J. & Schneider, R.R. 1993. An automated leaching method for the determination of opal in sediments and particulate matter. *Deep-Sea Research I*, **40**, 425–444.

ODP Leg 178 Shipboard Scientific Party 1999. Site 1095. *In* Barker, P.F., Camerlenghi, A., Acton, G.D. & Ramsay, A.T.S., *eds*. *Proceedings of the Ocean Drilling Program, Scientific Results*, **178**, 1–173.

O'Grady, D.B. & Syvitski, J.P.M. 2001. Predicting profile geometry of continental slopes with a multi-process sedimentation model. *In* Merriam, D.F. & Davis, J.C., *eds. Geologic modeling and simulation: sedimentary systems*. New York: Springer, 99–117.

Pudsey, C.J. 2002. Neogene record of Antarctic Peninsula glaciation in continental rise sediments: ODP Leg 178, Site 1095. *In* Barker, P.F., Camerlenghi, A., Acton, G.D. & Ramsay, A.T.S., *eds*. *Proceedings of the Ocean Drilling Program, Scientific Results*, **178**, 1–25.

Pudsey, C.J. & Camerlenghi, A. 1998. Glacial-interglacial deposition on a sediment drift on the Pacific margin of the Antarctic Peninsula. *Antarctic Science*, **10**, 286–308.

Rabouille, C., Gaillard, J.-F., Treguer, P. & Vincendeau, M.-A. 1997. Biogenic silica recycling in surficial sediments across the Polar Front of the Southern Ocean (Indian Sector). *Deep-Sea Research II*, **44**, 1151–1176.

Ragueneau, O., Tréguer, P., Leynaert, A., Anderson, R.F., Brzezinski, M.A., DeMaster, D.J., Dugdale, R.C., Dymond, J., Fischer, G. & François, R. 2000. A review of the Si cycle in the modern ocean: Recent progress and missing gaps in the application of biogenic opal as a paleoproductivity proxy. *Global and Planetary Change*, **26**, 317–365.

Raymond, C.F. 2002. Ice sheets on the move. *Science*, **298**, 2147–2148.

Rebesco, M.A., Larter, R.D., Camerlenghi, A. & Barker, P.F. 1996. Giant sediment drifts on the continental rise west of the Antarctic Peninsula. *Geo-Marine Letters*, **16**, 65–75.

Rebesco, M.A., Pudsey, C.J., Canals, M., Camerlenghi, A., Barker, P.F., Estrada, F. & Giorgetti, A. 2002. Sediment drifts and deep-sea channel systems, Antarctic Peninsula Pacific Margin. *Geological Society of London Memoirs*, **22**, 353–371.

Rebesco, M. & Camerlenghi, A. 2008. Late Pliocene margin development and mega debris flow deposits on the Antarctic continental margins: Evidence of the onset of the modern Antarctic Ice Sheet? *Palaeogeography, Palaeoclimatology, Palaeoecology*, **260**, 149–167.

Schlüter, M. 1990. *Early diagenesis of organic carbon and opal in sediments of the southern and eastern Weddell Sea: geochemical analysis and modelling*. PhD thesis, Alfred Wegener Institut für Polar- und Meeresforschung, Bremerhaven, 156 pp.

Stein, R. 1990. Organic carbon content/sedimentation rate relationship and its paleoenvironmental significance for marine sediments. *Geo-Marine Letters*, **10**, 37–44.

Stow, D.A.V. 1986. Deep clastic seas. *In* Reading, H.G., *ed. Sedimentary environments and facies*. Oxford: Blackwell Scientific, 399–444.

Stow, D.A.V. & Mayall, M. 2000. Deep-water sedimentary systems: new models for the 21st century. *Marine and Petroleum Geology*, **17**, 125–135.

Treguer, P., Nelson, D.M., Van Bennekom, A.J., DeMaster, D.J., Leynaert, A. & Queguiner, B. 1995. The silica balance in the world ocean: a reestimate. *Science*, **268**, 375–379.

Uenzelmann-Neben, G. 2006. Depositional patterns at Drift 7, Antarctic Peninsula: along-slope versus down-slope sediment transport as indicators for oceanic currents and climatic conditions. *Marine Geology*, **233**, 49–62.

Van Der Weijden, A.J. & Van Der Weijden, C.H. 2002. Silica fluxes and opal dissolution rates in the northern Arabian Sea. *Deep-Sea Research I*, **49**, 157–173.